# Hyperfine excitation of 13CCH and C13CH by collisions with para- H2

P Pirlot Jankowiak, F Lique, P J Dagdigian

MNRAS 000, 1–9 (2023) Preprint 31 May 2023 Compiled using MNRAS LATEX style file v3.0

# Hyperfine excitation of $^{13}$CCH and C$^{13}$CH by collisions with *para*-$H_2$

P. Pirlot Jankowiak,[1] F. Lique,[1]★ and P. J. Dagdigian[2]
[1]*Univ Rennes, CNRS, IPR (Institut de Physique de Rennes) - UMR 6251, F-35000 Rennes, France*
[2]*Department of Chemistry, The Johns Hopkins University, Baltimore, MD 21218-2685, USA*

Accepted XXX. Received YYY; in original form ZZZ

**ABSTRACT**

The computation of hyperfine resolved cross sections and rate coefficients for open-shell molecules in collision with $H_2$ is a true methodological and numerical challenge. Such collisional data are however required to interpret astrophysical observations. We report the first hyperfine resolved rate coefficients for (de-)excitation of $^{13}$CCH and C$^{13}$CH isotopologues induced by collisions with *para*-$H_2$. These calculations have been performed using a recently published $C_2H$–$H_2$ potential energy surface. Hyperfine resolved cross sections and rate coefficients between the first 98 energy levels of the two isotopologues were determined using a recoupling technique for temperatures ranging from 5 to 100 K. Significant isotopic substitution effects were found, showing the necessity of computing isotopologue specific collisional data. These rate coefficents have then been used in a simple radiative transfer modeling for typical molecular cloud conditions.

**Key words:** molecular data – molecular processes – radiative transfer

## 1 INTRODUCTION

Among the hydrocarbons detected in the interstellar medium (ISM), the ethynyl radical ($C_2H$) is one of the most abundant. The first detection of this radical has been reported by Tucker et al. (1974) in 13 galactic sources through hyperfine resolved observations of its rotational emission line $n = 1 \rightarrow 0$, prior its study in laboratory (Sastry et al. 1981). This identification was confirmed later by Ziurys et al. (1982) with the detection of the $n = 3 \rightarrow 2$ emission line. This radical has been observed over the past decades in several astrophysical environments including prestellar cores (Padovani et al. 2009), photodissociated regions (Teyssier et al. 2003; Cuadrado et al. 2015), protoplanetary disks (Dutrey et al. 1996), high mass star forming regions (Beuther et al. 2008) and dark clouds (Sakai et al. 2010).

The high abundance of $C_2H$ in the ISM made also possible the detection of its carbon-based isotopologues $^{13}$CCH and C$^{13}$CH. Indeed, Salek et al. (1994) detected them through hyperfine resolved observations of the $n = 2 \rightarrow 1$ and $n = 1 \rightarrow 0$ rotational lines respectively. Observations of the $^{13}$C isotopologues can provide interesting insight into the formation path of $C_2H$ and the [$^{12}$C/$^{13}$C] isotopic fractionation in the ISM.

It has been shown that this [$^{12}$C/$^{13}$C] ratio in $C_2H$ isotopologues deviates from the [$^{12}$C/$^{13}$C] = 60 elemental value (Lucas & Liszt 1998), depending on environments and on the isotopologues. Sakai et al. (2010) derived [CCH/$^{13}$CCH] and [CCH/C$^{13}$CH] ratios higher than 170 and 250 in TMC-1 and higher than 80 and 135 in L1527. Additionnally, these authors found a [C$^{13}$CH/$^{13}$CCH] ratio to be 1.6 in both sources. Such behaviour have been also found by Salek et al. (1994) and later by Cuadrado et al. (2015); Taniguchi et al. (2019); Yoshida et al. (2019).

Sakai et al. (2010) suggest that the [C$^{13}$CH/$^{13}$CCH] ratio might be due to the different production mechanisms of $C_2H$ in cold environments, especially that the two carbons are not equivalent in its pathway through neutral-neutral reactions, or to exchange reactions between $^{13}$CCH and C$^{13}$CH after their formation through the following process:

$$^{13}\mathrm{CCH} + \mathrm{H} \rightleftarrows \mathrm{C}^{13}\mathrm{CH} + \mathrm{H} + \Delta E_1$$

where $\Delta E_1 \sim 8$ K corresponds to the difference of the zero-point energy of $^{13}$CCH with respect to C$^{13}$CH. The detection of the isotopologues by Cuadrado et al. (2015) in the Orion Bar PDR suggests also that reactions with $^{13}C^+$ can explain the observed fractionation in warmer objects through processes such as

$$^{13}\mathrm{C}^+ + \mathrm{CCH} \rightleftarrows \mathrm{C}^{13}\mathrm{CH} + \mathrm{C}^+ + \Delta E_2$$
$$^{13}\mathrm{C}^+ + \mathrm{CCH} \rightleftarrows {}^{13}\mathrm{CCH} + \mathrm{C}^+ + \Delta E_3$$

where $\Delta E_2 \sim 63$ K and $\Delta E_3 \sim 55$ K are the differences of zero point energy of both isotopologues with respect to $C_2H$.

In the ISM, especially in cold environments, the density is low, and the populations of molecular levels do not follow a Maxwell-Boltzmann distribution. This non-local thermal equilibrium (non-LTE) behaviour implies a competition between radiative and collisional processes in these environments. Radiative transfer modeling, to interpret the observed spectroscopic intensities, requires then both radiative and collisional data for the observed molecules. While Einstein coefficients depend on the dipole moment and the energetic structure of the molecule that can be found in databases, rate coefficients must be computed through scattering calculations for each collisional system. These calculations require the prior determination of the potential energy surface (PES) through *ab initio* calculations

★ E-mail: francois.lique@univ-rennes.fr

describing the electronic interaction of the observed molecules with the main collider in molecular clouds, generally $H_2$.

To the best of our knowledge, there are no collisional data for collisions of $^{13}$CCH and C$^{13}$CH. Indeed, the determination of hyperfine resolved rate coefficients of $^{13}$CCH and C$^{13}$CH in collision with $H_2$ is a true computational challenge. The coupling of the two nonzero nuclear spins of both the $^{13}$C and H atoms to the molecular rotation of $C_2H$ isotopologues leads to a large number of hyperfine energy levels. Scattering calculations with the $H_2$ collider would imply a very large number of coupled channels to include, and such calculations would overly tax current computational resources. Because of this lack of collisional data, scaled HCN–He collisional data from Green & Thaddeus (1974) have been used by Sakai et al. (2010), including the hyperfine structure of $C_2H$ isotopologues through Infinite Order Sudden (IOS) scaling techniques for non-LTE analysis of $^{13}$CCH and C$^{13}$CH observations. At the present time, the same scaling techniques can be applied on $C_2H$–$H_2$ data but isotopic substitution effect have been shown to be non negligible (Dumouchel et al. 2017).

Presently, hyperfine scattering calculations of molecule-molecule collisions involving only one nuclear spin are feasible in terms of CPU time and memory. Such studies have been performed using the recoupling method for the OH/OD–$H_2$ (Offer et al. 1993; Kłos et al. 2020; Dagdigian 2021), $SH^+$–$H_2$ (Dagdigian 2019) and $C_2H$–$H_2$ (Dagdigian 2018b) collisional systems. For molecules with two nonzero nuclear spins, a few investigations have been carried out using the recoupling method, considering the projectile as a structureless collider for the NH/ND–He (Dumouchel et al. 2012), $C_3N$–He (Lara-Moreno et al. 2021) and $N_2H^+$–He (Daniel et al. 2005) systems.

The purpose of this paper is to overcome this challenging problem and provide accurate hyperfine rate coefficients of $^{13}$CCH and C$^{13}$CH in collisions with $H_2$ for temperatures up to 100 K. To do so, two approaches (recoupling based methods and IOS) will be considered. Since $^{13}$CCH and C$^{13}$CH have been detected mostly in cold molecular clouds, it can be assumed that at the low temperature of the clouds only *para*-$H_2$ in its ground rotational state ($j_2 = 0$, $j_2$ being the rotational state of $H_2$) is populated.

This paper is organized as follow: The methodology and especially the selection of a suitable scattering approach are presented in section 2. Then, a presentation of the features of the $C_2H$–$H_2$ PES used in this work is given with also a description of the transformation of the $C_2H$–$H_2$ PES to consider isotopic substitution. Section 3 presents and compares the hyperfine rate coefficients for the $C_2H$ isotopologues in collision with $H_2$. An application to radiative transfer modeling is carried out in section 4. This paper follows with a conclusion in section 5.

## 2 METHODOLOGY

### 2.1 Energy levels of $C_2H$ and $^{13}$C isotopologues

$C_2H$ is a radical with a $^2\Sigma^+$ ground electronic state. Its rotational levels are split by the spin-rotation interaction. The corresponding angular momentum $j$ can be defined by

$$\mathbf{j} = \mathbf{n} + \mathbf{S}$$

where $n$ is the nuclear rotational angular momentum and $S = 1/2$ the electronic spin. The presence of nonzero nuclear spin for the H [$I$(H) = 1/2] atom involves a coupling of the nuclear spin with the angular momentum $j$. Thus, the hyperfine splitting in $C_2H$ is described by the $F$ quantum number where

$$\mathbf{F} = \mathbf{j} + \mathbf{I(H)}$$

Since the $^{13}$CCH and C$^{13}$CH isotopologues possess the same electronic structure as $C_2H$, they have a similar fine structure, with just slight differences in the spectroscopic constants. However, both H and $^{13}$C atoms have nonzero nuclear spins which couple to the rotation. The hyperfine coupling scheme can now be described as

$$\mathbf{F}_1 = \mathbf{j} + \mathbf{I(H)}, \quad \mathbf{F} = \mathbf{F}_1 + \mathbf{I(^{13}C)}$$

where $F_1$ and $F$ now label the hyperfine levels. The nuclear spin of the $^{13}$C nucleus equals $I(^{13}\mathrm{C}) = 1/2$. The energy levels have been taken from the CDMS database (Endres et al. 2016). For $^{13}$C isotopologues, each rotational level ($n > 1$) is split in 8 hyperfine components except $n = 0$ and 1 which are split in 3 and 7 levels respectively (see Table 1).

**Table 1.** The lower hyperfine energy levels of $^{13}$CCH and C$^{13}$CH

| Level | $n$ | $j$ | $F_1$ | $F$ | $E$ (cm$^{-1}$) | |
|---|---|---|---|---|---|---|
| | | | | | $^{13}$CCH | C$^{13}$CH |
| 1 | 0 | 0.5 | 0 | 0.5 | 0.000000 | 0.000000 |
| 2 | 0 | 0.5 | 1 | 0.5 | 0.029385 | 0.0004836 |
| 3 | 0 | 0.5 | 1 | 1.5 | 0.030483 | 0.005863 |
| 4 | 1 | 1.5 | 1 | 0.5 | 2.806987 | 2.843558 |
| 5 | 1 | 1.5 | 1 | 1.5 | 2.807052 | 2.843867 |
| 6 | 1 | 1.5 | 2 | 1.5 | 2.835465 | 2.847896 |
| 7 | 1 | 1.5 | 2 | 2.5 | 2.836402 | 2.848807 |
| 8 | 1 | 0.5 | 0 | 0.5 | 2.83746 | 2.850608 |
| 9 | 1 | 0.5 | 1 | 0.5 | 2.838841 | 2.851297 |
| 10 | 1 | 0.5 | 1 | 1.5 | 2.83932 | 2.851413 |
| 11 | 2 | 2.5 | 2 | 1.5 | 8.420948 | 8.530995 |
| 12 | 2 | 2.5 | 2 | 2.5 | 8.421056 | 8.531445 |
| 13 | 2 | 2.5 | 3 | 2.5 | 8.448568 | 8.534911 |
| 14 | 2 | 2.5 | 3 | 3.5 | 8.449434 | 8.535765 |
| 15 | 2 | 1.5 | 2 | 1.5 | 8.452741 | 8.539588 |
| 16 | 2 | 1.5 | 2 | 2.5 | 8.45246 | 8.53980 |
| 17 | 2 | 1.5 | 1 | 1.5 | 8.453786 | 8.540354 |
| 18 | 2 | 1.5 | 1 | 0.5 | 8.453825 | 8.540546 |

### 2.2 Selection of suitable approach for scattering calculations: validation with the $C_2H$–$H_2$ collisional system

Excitation in molecule-molecule collisions involving an open-shell molecule is a computational challenge. Indeed, the presence of fine and hyperfine structure can lead to a large number of energy levels to take into account in scattering calculations. Especially, when these molecules possess more than one nonzero nuclear spin, quantum calculations are almost not doable since hyperfine resolved cross sections require a large number of coupled channels to take into account.

The purpose of this paper is to provide hyperfine resolved collisional data for $^{13}$CCH and C$^{13}$CH with $H_2$ using nuclear spin-free $S$-matrices. In order to choose the most suitable method to perform such intensively demanding calculations, comparison of both reduced dimension recoupling (Alexander & Dagdigian 1985; Corey & McCourt 1983; Offer et al. 1993) and IOS (Faure & Lique 2012) methods will be performed on the $C_2H$–$H_2$ collisional system.

In the case of the IOS approximation, nuclear spin-free cross sections and rate coefficients have been calculated with the 4D PES from Dagdigian (2018b) and taking into account the inclusion of the rotational levels of $H_2$ $j_2 = 0$ and 2, in the scattering basis. IOS hyperfine resolved rate coefficients are determined using the correction of Neufeld & Green (1994) $\left(k^{\rm NG}_{njF\rightarrow n'j'F'}\right)$ described in Appendix A.

For the reduced dimension approach, nuclear spin-free cross sections were computed by reducing the dimension of the $C_2H$–$H_2$ 4D PES of Dagdigian (2018a) to 2D. To do so, we restrict the $l_2$ index to zero [see Eq 3 and text below for details]. This is equivalent of restricting the $H_2$ scattering basis to $j_2 = 0$. Hyperfine cross sections are then computed through the recoupling method. Rate coefficients $\left(k^{\rm 2D-rec}_{njF\rightarrow n'j'F'}\right)$ from an initial level $i$ to a final level $f$ were determined by integrating the cross sections over a Maxwell-Boltzmann distribution over the collisional energies $E_c$:

$$k_{i\rightarrow f}(T) = \left(\frac{8}{\pi\mu(k_BT)^3}\right)^{1/2}\int_0^\infty \sigma_{i\rightarrow f}(E_c)E_c e^{-E_c/k_BT}dE_c \quad (1)$$

These two approaches will be compared with the full calculations (Dagdigian 2018b) for the $C_2H$–$H_2$ collisional system.[1] These data $\left(k^{\rm 4D-rec}_{njF\rightarrow n'j'F'}\right)$ have been taken as the reference.

Hyperfine cross sections are determined up to total energies of 500 cm$^{-1}$; this ensures convergence of the rate coefficients up to 50 K, for levels up to $n = 7$. Spectroscopic constants were taken from Gottlieb et al. (1983) and the reduced mass $\mu = 1.865$ amu. All calculations have been performed using the HIBRIDON scattering code (Alexander et al. 2023).

Fig. 1 presents a comparison at 10 K and 50 K of 2D and scaled IOS $C_2H$–$H_2$ hyperfine rate coefficients with those computed with the 4D PES and the recoupling approach. The dashed lines represent deviations of the rate coefficients within a factor of 2. One can see that the 2D rate coefficients are almost systematically overestimating the 4D ones by $\sim 20\%$, whereas the scaled IOS data are spread up to a factor of 2 for some transitions, despite the fact that the dominant transitions are however well reproduced.

It is possible to quantify better the deviations of the results by computing the weighted mean error factor (WMEF) such as (Loreau et al. 2018)

$$\mathrm{WMEF} = \frac{\sum_{\rm i,f} k^{\rm 4D-rec}_{\rm i\rightarrow f}\mathrm{r_i}}{\sum_{\rm i} k^{\rm 4D-rec}_{\rm i}} \quad (2)$$

where $k_i^{\rm 4D-rec}$ is the rate coefficient for the $i^{th}$ transition computed with the 4D PES and using the recoupling technique and $r_i = \max(k_i^{\rm 4D-rec}/k^{\rm 2D/NG}, k^{\rm 2D/NG}/k_i^{\rm 4D-rec})$ so that $r_i \geq 1$. Taking this quantity into account, both approaches have a very similar WMEF. Especially in the case of the IOS approximation, the largest transitions ($> 10^{-11}$ cm$^3$ s$^{-1}$) are almost matching perfectly the corresponding 4D transitions.

None of these methods seems to stand out more than another, and it was assumed that these differences would be the same for the study of the $^{13}$C isotopologues. Then, for the next step of this work, hyperfine rate coefficients of $^{13}$CCH and C$^{13}$CH with $H_2$ will be computed using the reduced dimension approach. Several arguments tend to explain this choice:

[1] An error of a factor $\sim 1.4$ has been found in these computed rate coefficients and has been corrected

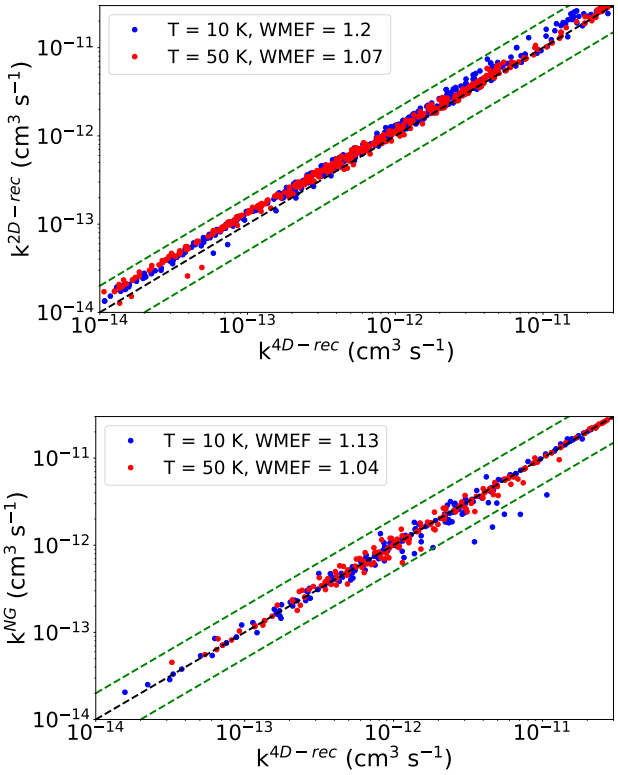


**Figure 1.** Systematic comparison at 10 K and 50 K of $C_2H$–*sph*-$H_2$ recoupling hyperfine rate coefficients with $C_2H$–*para*-$H_2$ ones (upper panel) and corrected IOS hyperfine rate coefficients with $C_2H$–*para*-$H_2$ ones (lower panel). The green dashed lines represent deviations of the rate coefficients within a factor of 2

i) According to Fig. 1, the quantification of the deviation is better defined for the 2D approach since deviations are more systematic.

ii) From a theoretical point of view, there is only one approximation made with the 2D approach (neglecting the structure of $H_2$ and the corresponding coupling terms in the PES), whereas IOS approximation is subject to additional approximations: neglect of the rotational structure of the target, scaling relation based on the assumption of a similar error between IOS and Close-Coupling (CC) to describe rate coefficients among relative hyperfine levels. Also, the correction of Neufeld & Green (1994) requires the calculation of elastic cross sections in order to predict quasi-elastic hyperfine transitions ($n = n', j = j', F \neq F'$). However, CC elastic cross sections are usually not fully converged, and a scaled application of IOS limit is not able to provide quasi-elastic transitions properly. One should note that in Fig. 1, some rate coefficients higher than $3 \times 10^{-12}$ cm$^3$ s$^{-1}$ deviate more than a factor of 2. They are related to quasi-elastic transitions, which can only be extrapolated through pure IOS calculations.

iii) The reduced dimension approach leads to a reasonable error according to astrophysical modeling. The use of the IOS approach would have been more suitable if there was a strong dependance of the orientation of $H_2$ in the cross sections as in the case for NH–$H_2$ collisions (Pirlot Jankowiak et al. 2021) where taking only $j_2 = 0$ leads to a mean error of 40%.

### 2.3 The excitation of $^{13}$C isotopologues

#### *2.3.1 Potential energy surface*

$C_2H$ and its isotopologues differ only by the composition of their nucleus and have the same electronic structure. Then, through the Born-Oppenheimer approximation, it is possible to use the $C_2H$–$H_2$ PES to describe the interaction of $^{13}$CCH and C$^{13}$CH with molecular hydrogen. The $C_2H$–$H_2$ interaction potential has been computed by one of the authors (Dagdigian 2018a). This author used the restricted coupled cluster method with single, double and (perturbative) triple excitations [RCCSD(T)] (Knowles et al. 1993) with the aug-cc-pVQZ basis set. $C_2H$ has a linear geometry, and the PES has been determined assuming that $C_2H$ and $H_2$ have rigid structures, with their bond lengths taken as the average value of their respective ground vibrational states.

In order to be suitable for time-independent scattering calculations, the analytical representation of the potential has been given in terms of an expansion in bispherical harmonics $A_{l_1 l_2 l}(\theta_1, \theta_2, \phi)$:

$$V(R, \theta_1, \theta_2, \phi) = \sum_{l_1 l_2 l} v_{l_1 l_2 l}(R) A_{l_1 l_2 l}(\theta_1, \theta_2, \phi) \tag{3}$$

where

$$A_{l_1 l_2 l}(\theta_1, \theta_2, \phi) = \left[\frac{(2l+1)}{4\pi}\right]^{1/2} \sum_m (l_1 m l_2, -m|l0) \times Y_{l_1 m}(\theta_1, 0) Y_{l_2, -m}(\theta_2, \phi) \tag{4}$$

Here, the intermolecular distance between the centers of mass of $C_2H$ and $H_2$ is represented by the Jacobi vector **R**, $\theta_1$ is the angle between $C_2H$ molecular axis and **R** (with the carbon end of $C_2H$ pointing toward $H_2$ for $\theta_1 = 0$), $\theta_2$ is the angle between $H_2$ molecular axis and **R**, and $\phi$ is the dihedral angle. The terms $v_{l_1 l_2 l}(R)$ are the expansion coefficients of the potential for a given intermolecular separation $R$, $l_1$, $l_2$ are the expansion indexes for $C_2H$ and $H_2$ respectively and $l$ was selected as $|l_1 - l_2| < l < l_1 + l_2$.

The transformation of the $C_2H$–$H_2$ PES to the $^{13}$CCH or C$^{13}$CH–$H_2$ PES requires a shift of the origin of their center of mass $\delta r$. The centers of mass are shifted by $-0.049 a_0$ for $^{13}$CCH and $+0.039 a_0$ for C$^{13}$CH. The negative value means that the shift is toward the carbon end, and positive if the shift is toward the hydrogen end (see Fig. 2). The "+/-" notation represents the coordinates in the corresponding isotopologue frame. Then, the transformation of the Jacobi coordinates takes the form

$$\delta r^{+/-} = r(\mathrm{C^{13}CH}/^{13}\mathrm{CCH}) - \mathrm{r(C_2H)} \tag{5}$$

$$R^{+/-} = \sqrt{R^2 + \delta r^2 + 2R\delta r^{+/-} \cos(\theta_1)} \tag{6}$$

$$\theta_1^{+/-} = \arcsin\left(\frac{R \sin(\theta_1)}{R^{+/-}}\right) \tag{7}$$

The transformation of angles describing $H_2$ orientation $(\theta_2, \phi)$ has been neglected since $H_2$ will be considered as a pseudo-structureless projectile (see the discussion in the following paragraphs). The shift of the center of mass implies a new expansion of the potential for the interaction of the isotopologues with $H_2$. This has been carried out in this work using a Gauss-Legendre quadrature with 686 different geometries in order to obtain 174 coefficients up to $l_1 = 12$ and $l_2 = 6$ to be consistent with the number of coefficients employed by Dagdigian (2018a).

In order to model $H_2$ as a pseudo atom, a reduction of the dimensionality of the PES was performed so that only *para*-$H_2$ ($j_2 = 0$) is involved as a collider (hereafter *sph*-$H_2$). One can simplify equation (3) using only terms where $l_2 = 0$. This simplification yields the following form for the potential appropriate to treating collisions of a $^2\Sigma^+$ molecule with a (pseudo)atom:

$$V(R, \theta_1) = \sum_{l_1} \left(\frac{[l_1]}{4\pi^{3/2}}\right) v_{l_1 0 l_1} P_{l_1}(\cos\theta_1) \tag{8}$$

with $[l_1] \equiv 2l_1 + 1$. Then, instead of 174 expansion coefficients, only 13 coefficients are needed for the CC calculations. This transformation is used to determine hyperfine cross sections through the recoupling method, as described in Sec. 2.3.2. The lower-order expansion coefficients are presented in Fig. 3.

Most of the coefficients are very close for all three ($C_2H$, $^{13}$CCH and C$^{13}$CH) isotopologues interacting with $H_2$. Slight differences can be seen for odd $l_1$ indexes, especially for $l_1 = 1$, where the repulsive behaviour is dominant for $^{13}$CCH. Since the shift of the center of mass is closer to the edge of the molecule, this term characterizes a larger odd anisotropy for the $^{13}$CCH–$H_2$ potential.

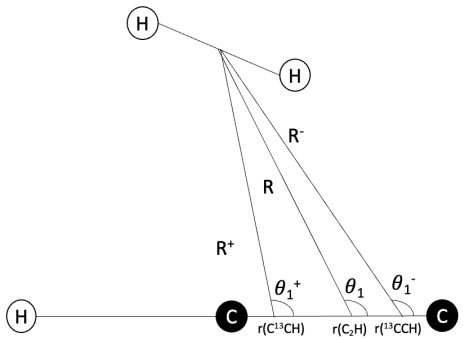


**Figure 2.** Representation of the $C_2H$–$H_2$, $^{13}$CCH-$H_2$ and C$^{13}$CH-$H_2$ interactions in Jacobi coordinates

#### *2.3.2 Scattering formalism: the recoupling method*

With the reduction to two nuclear degrees of freedom, the formalism of atom-molecule collisions with two nonzero nuclear spins can be readily applied. It should be noted that the recoupling method is rigorous if the hyperfine splittings are negligible compared to the rotational energy spacings.

In the recoupling method, the $T$-matrix elements for a molecule-(pseudo)atom collision with inclusion of the nuclear spins can be obtained from the nuclear spin-free $T$-matrix elements as described below. The total angular momentum $\mathbf{J_H}$ of the complex when the H nuclear spin is included equals $\mathbf{J} + \mathbf{I(H)}$, where $\mathbf{J}$ is the total angular momentum of the complex without the H nuclear spin. In this case, the $T$-matrix element is given by (Corey & McCourt 1983)

$$T^{J_H}_{n'j'F_1'L',njF_1L} = (-1)^{j'-j+L'-L} \sum_J [J] \times \begin{Bmatrix} I(\mathrm{H}) & j & F_1 \\ L & J_H & J \end{Bmatrix} \begin{Bmatrix} I(\mathrm{H}) & j' & F_1 \\ L' & J_H & J \end{Bmatrix} T^J_{n'j'L',njL} \tag{9}$$

where $[x] = 2x + 1$. The nuclear spin $\mathbf{I(H)}$ equals 1/2.

We now apply a second recoupling to include the $^{13}$C nuclear spin. The total angular momentum $\mathbf{J_T}$ of the complex when both nuclear spins are included equals $\mathbf{J_H} + \mathbf{I}(^{13}\mathbf{C})$. We note that $\mathbf{I}(^{13}\mathbf{C})$ equals

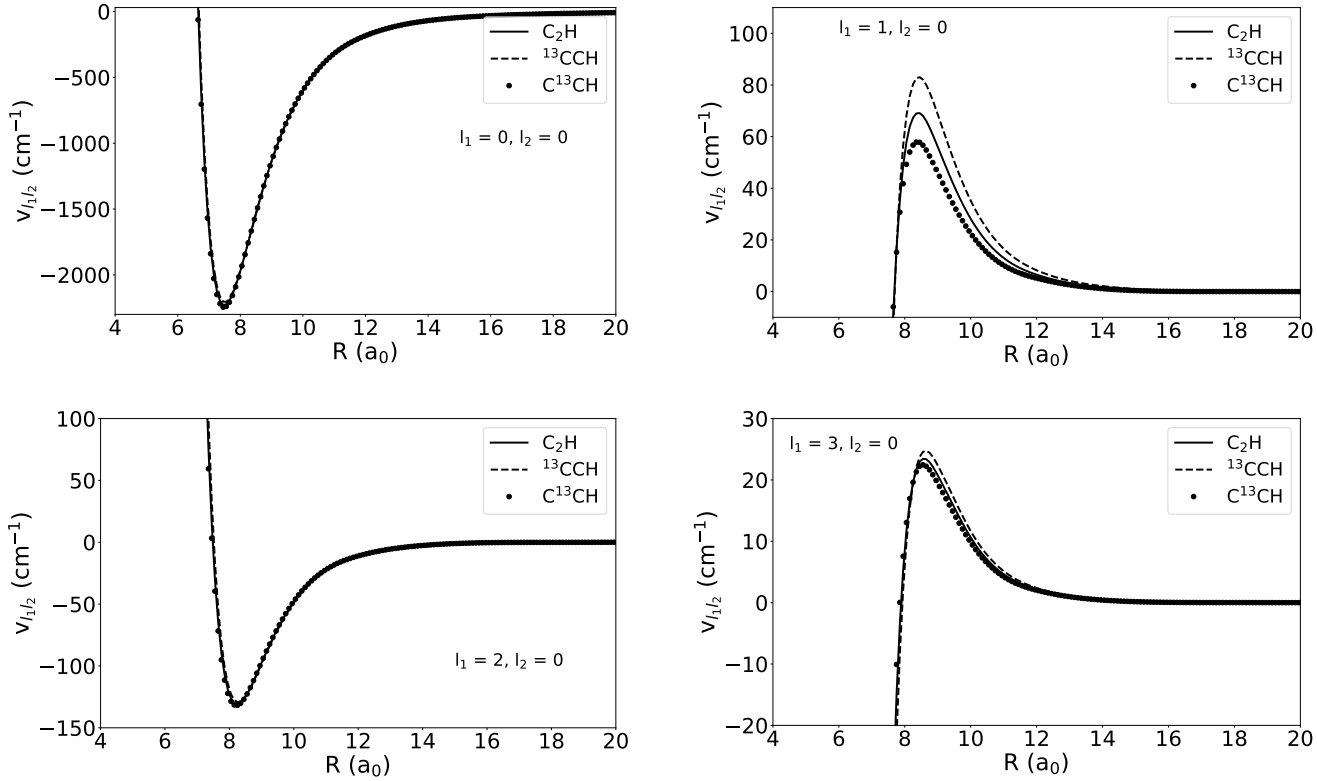


**Figure 3.** Radial dependence of the lower-order expansion coefficients for $C_2H$ and isotopologues interaction with $H_2$. Solid lines are apply to $C_2H$, dashed lines to $^{13}$CCH and dotted lines to C$^{13}$CH.

1/2. The $T$-matrix element in this case can be written as

$$T^{J_T}_{n'j'F'F'_1L',njFF_1L} = (-1)^{F'-F+L'-L} \sum_{J_H} [J_H] \times \begin{Bmatrix} I(^{13}C) & F_1 & F \\ L & J_T & J_H \end{Bmatrix} \begin{Bmatrix} I(^{13}C) & F'_1 & F \\ L' & J_T & J_H \end{Bmatrix} \times T^{J_H}_{n'j'F'_1L',njF_1L} \quad (10)$$

The hyperfine cross sections may be calculated with the $T$-matrix elements given in Eq. 10:

$$\sigma_{n'j'F'_1F'\rightarrow njF_1F} = \frac{\pi}{k^2[F]} \sum_{J_T} [J_T] |T^{J_T}_{n'j'F'F'_1L',njFF_1L}|^2 \quad (11)$$

Lara-Moreno et al. (2021) have carried out the equivalent calculation using $12j$ symbols of the second kind. In fact, this $12j$ symbol is defined as the product of four $6j$ symbols, similar to those seen in Eqs. 9 and 10.

## 3 $^{13}$CCH–$H_2$ AND C$^{13}$CH–$H_2$ RATE COEFFICIENTS

Scattering calculations have been carried out for the 98 first $^{13}$CCH and C$^{13}$CH hyperfine levels up to $n$ = 12 and for a total energy up to $E$ = 1370 cm$^{-1}$. Details about scattering parameters are given in Appendix B. Rate coefficients have been computed up to 100 K to cover the range of temperatures where these species are observed. Scattering calculations have been performed using the HIBRIDON software (Alexander et al. 2023).

Fig. 4 presents the temperature variation of several state-to-state hyperfine rate coefficients for $^{13}$CCH–*sph*-$H_2$ and C$^{13}$CH–*sph*-$H_2$ collisional systems. One can see a strong propensity rule for $\Delta n = \Delta j = \Delta F_1 = \Delta F$ transitions. The smallest rate coefficients are characterized by $\Delta n \neq \Delta j$. These trends have been already found before by Flower & Lique (2015) for $^{13}$CN and C$^{15}$N in collision with *para*-$H_2$. A similar behaviour is also observed in the case of NH/ND–He (Dumouchel et al. 2012) in the case of two nuclear spins. The $\Delta F = \Delta j$ propensity rule (Alexander & Dagdigian 1985) is also highlighted for open-shell molecules with one nuclear spin such as $C_2H/C_2D$–$H_2$ (Dumouchel et al. 2017; Dagdigian 2018b) or CN–$H_2$ (Kalugina et al. 2012). This propensity rule is a consequence of the fact that the nuclear spin is a spectator in the collision.

In addition, a general trend is that almost all hyperfine transitions for $^{13}$CCH–*sph*-$H_2$ collisional system are greater than the ones for the C$^{13}$CH–*sph*-$H_2$ collisional system. This behaviour mostly comes from the shift of the center of mass toward the edge of the molecule, leading to a greater anisotropy in the interaction of $^{13}$CCH with $H_2$ (see Fig. 2). Indeed, this effect looks systematic as one can see in Fig. 5. The differences are estimated within a factor 1.5, which is higher than the observed errors between the methodologies compared in Sec 2.2. Also, these differences are relatively high regarding the small shift of the center of mass and the similarity of their rotational constants [$B(^{13}CCH)$ = 1.404 cm$^{-1}$ and $B$(C$^{13}$CH) = 1.422 cm$^{-1}$] (McCarthy et al. 1995).

It is also interesting to investigate the impact of the isotopic substitution against the main isotopologue $C_2H$. Since $^{13}$CCH, C$^{13}$CH and $C_2H$ do not have the same hyperfine structure, the discussion will focus on the fine-structure excitation of these molecules with *sph*-$H_2$ to keep results on the same level of theory.

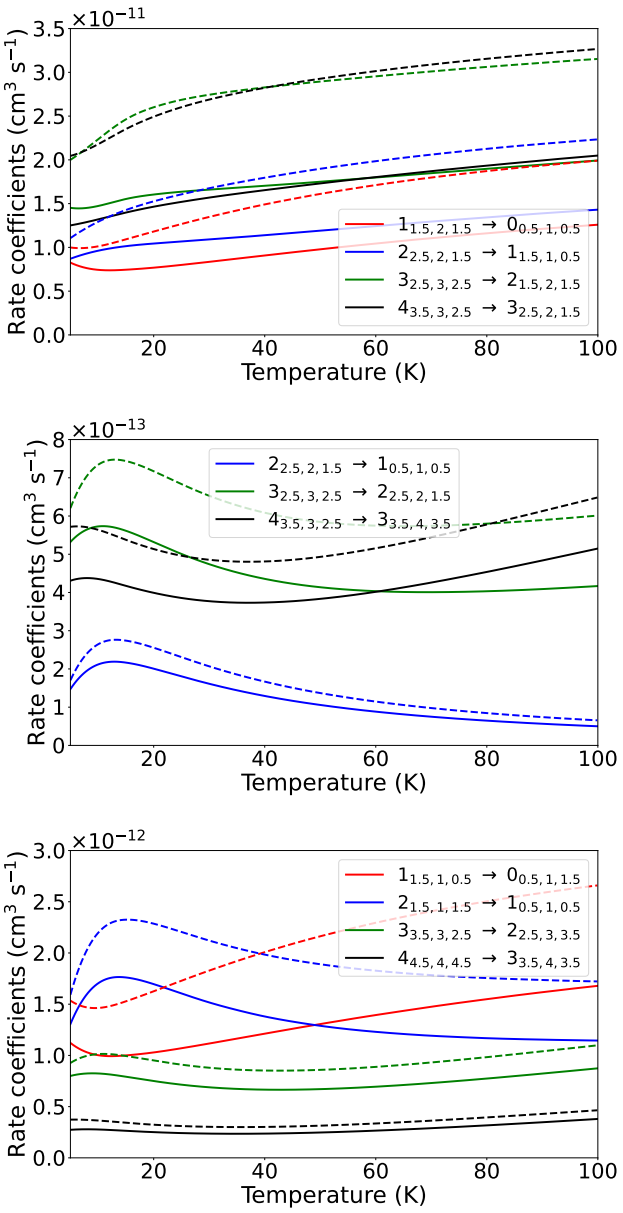


**Figure 4.** Temperature dependence of $^{13}$CCH–*sph*-$H_2$ (dashed lines) and C$^{13}$CH–*sph*-$H_2$ (solid lines) hyperfine rate coefficients for $\Delta n = \Delta j$ (upper), $\Delta n \neq \Delta j$ (middle) and $\Delta F_1 = \Delta j \pm 1$ (lower) transitions

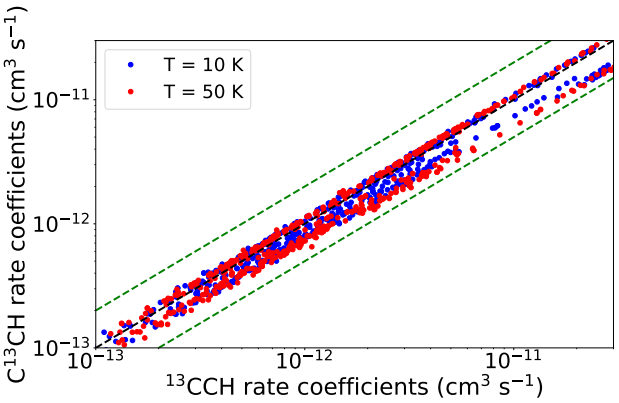


**Figure 5.** Comparison at 10 K and 50 K of hyperfine rate coefficients for all de-excitations of $^{13}$CCH–*sph*-$H_2$ and C$^{13}$CH–*sph*-$H_2$. The green dashed lines represent deviations of the rate coefficients within a factor of 2

## 4 ASTROPHYSICAL APPLICATION

With the present collisional data, it is possible to perform simple radiative transfer calculations. The aim is to check the possible impact of the isotopic substitution on radiative transfer modeling under non-LTE conditions. These calculations have been performed with the RADEX code (Van der Tak et al. 2007) using the escape probability approximation. In order to model astrophysical environments where these molecules are detected, such as TMC-1 (Sakai et al. 2010), L134N (Taniguchi et al. 2019) L1527 (Yoshida et al. 2019) or the Orion bar PDR (Cuadrado et al. 2015), kinetic temperatures were set at 10 K, 30 K and 50 K. The temperature of the background is set to 2.73 K to represent the cosmic microwave background (CMB). The column density is taken as $1 \times 10^{13}$ cm$^{-2}$, which is representative of the typical abundance of $C_2H$ isotopologues in cold molecular clouds. The line width is assumed to be 1 km s$^{-1}$. It is also assumed that the medium is cold enough so that only *para*-$H_2$ is populated. Then, explorations at $T_{\rm kin}$ = 50 K in the following paragraphs must be taken with caution since *ortho*-$H_2$ abundance is not negligible at this temperature. The Einstein coefficients $A_{ul}$ were taken from the CDMS database (Endres et al. 2016).

Excitation temperatures of observed hyperfine components of the $n = 1 \rightarrow 0$ line of $^{13}$CCH and C$^{13}$CH are plotted in Fig. 7 as a function of the *para*-$H_2$ density. As a general comment, all excitation temperatures strongly depend on the $H_2$ density, increasing from radiative (CMB temperature) to thermal equilibrium, where $T_{\rm ex} = T_{\rm kin}$. At $T_{\rm kin}$ = 10 K, one can see that relative differences of excitation temperatures of hyperfine transitions between the two isotopologues are very small, not exceeding 15%. However, for $T_{\rm kin}$ = 50 K, a weak maser effect is observed for transitions involving both isotopologues in the intermediate density range of $n_{\rm H_2} = 10^5 - 10^6$ cm$^{-3}$. One can notice in Fig. 8 a weak maser effect for excitation temperatures of C$^{13}$CH for the $n = 1$, $j = 0.5 \rightarrow n' = 0$, $j' = 0.5$ lines, whereas only a suprathermal effect is seen for $^{13}$CCH for the same transitions.

It is also interesting to look at the impact of the rate coefficients on the brightness temperature $T_{\rm B}$. Table 2 shows brightness temperatures for selected transitions at typical molecular cloud densities. The LTE modeling represents conditions where rate coefficients do not have influence anymore. Then, differences can only come from

Fig. 6 presents the temperature variation of fine-structure-resolved rate coefficients for the three collisional systems. The largest differences in the PES's appear for terms involving the $l_1 = 1$ expansion index, leading a larger odd anisotropy of the PES for $^{13}$CCH (see Fig. 3). Therefore, it is not surprising to observe larger rate coefficients for $^{13}$CCH–*sph*-$H_2$ than for $C_2H$–*sph*-$H_2$ and C$^{13}$CH–*sph*-$H_2$ for $\Delta n = \Delta j = 1$. It is interesting to note that rate coefficients look similar for $\Delta n = \Delta j = 2$ with a moderated inversion of behavior between $^{13}$CCH and C$^{13}$CH. It looks clear that $C_2H$ cannot be used as a substitute molecule for the other isotopologues.

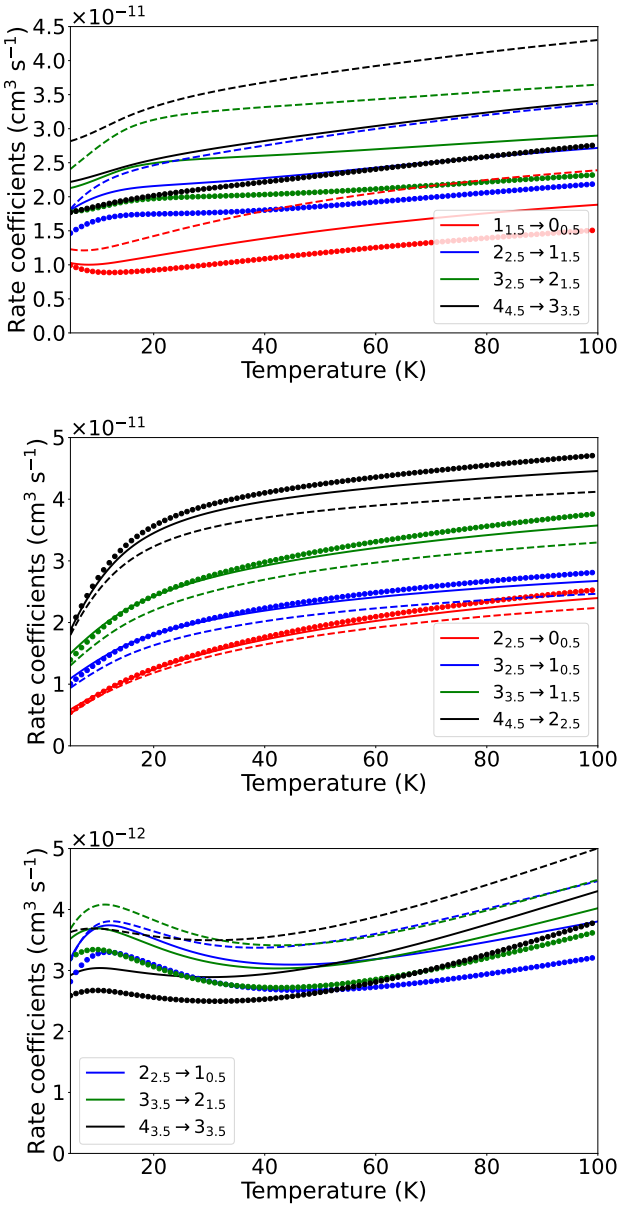


**Figure 6.** Temperature dependence of $C_2H$–*sph*-$H_2$ (solid lines), $^{13}$CCH–*sph*-$H_2$ (dashed lines) and C$^{13}$CH–*sph*-$H_2$ (dotted lines) hyperfine rate coefficients for $\Delta n = \Delta j = 1$ (upper), $\Delta n = \Delta j = 2$ (middle) and $\Delta n \neq \Delta j$ (lower) transitions

the magnitude of the Einstein coefficients and of the slight difference in the energy structure of the two isotopologues.

Even if brightness temperatures for all transitions are far from the LTE regime, differences between $^{13}$CCH and C$^{13}$CH remain very close to the ratio of the corresponding Einstein coefficients. Since rate coefficients for $^{13}$CCH-*sph*-$H_2$ are larger than for C$^{13}$CH-*sph*-$H_2$ ones, almost systematically $\frac{T_B(\mathrm{C}^{13}\mathrm{CH})}{T_B(^{13}\mathrm{CCH})} < \frac{A_{ul}(\mathrm{C}^{13}\mathrm{CH})}{A_{ul}(^{13}\mathrm{CCH})}$. However, these discrepancies are too low compared to the uncertainties in rate coefficients and astrophysical models to conclude on the possible impact of the isotopic substitution in the rate coefficients for the brightness temperature.

## 5 DISCUSSION & CONCLUSION

We have calculated hyperfine-resolved rate coefficients of $^{13}$CCH and C$^{13}$CH for collisions with $H_2$ including both nonzero nuclear spins of the H and the $^{13}$C nuclei. Hyperfine cross sections and rate coefficients have been carried out using the PES of Dagdigian (2018a) and the recoupling technique (Alexander & Dagdigian 1985).

Rate coefficients for $^{13}$CCH–*sph*-$H_2$ and C$^{13}$CH–*sph*-$H_2$ show a similar propensity rule in favor of $\Delta n = \Delta j = \Delta F_1 = \Delta F$ transitions. Transitions with larger rate coefficients are especially seen with $^{13}$CCH for $\Delta n = 1$ transitions, which is a direct consequence of the anisotropy of the PES with a shifted center of mass. $^{13}$CCH–*sph*-$H_2$ rate coefficients have been found to be generally larger than C$^{13}$CH–*sph*-$H_2$ ones within a factor 1.5. Even if this effect is moderate, it is still of importance regarding the small shift $|\delta r| = 0.04$-$0.05 a_0$ of the center of mass.

Finally, we carried out radiative transfer modeling using these sets of data. For modeling environments at $T_{\mathrm{kin}} = 10$ K, almost no differences have been found between $^{13}$CCH and C$^{13}$CH excitation temperatures of observed lines. However, maser effects are found for $^{13}$CCH and C$^{13}$CH at $T_{\mathrm{kin}} = 30$ K and 50 K. Brightness temperatures differ by a maximum of ∼10% from LTE conditions. Brightness temperatures ratios are almost systematically larger for C$^{13}$CH which is directly due to differences in the order of magnitude of the Einstein coefficients.

Then, the isotopic substitution does not have a significant impact on radiative transfer modeling and are not able to explain the [C$^{13}$CH/$^{13}$CCH] abundance ratio found in cold environments for the observed transitions (Sakai et al. 2010; Cuadrado et al. 2015; Taniguchi et al. 2019; Yoshida et al. 2019). One possible explanation would be that at very low temperature, the exchange reaction of the isotopic carbon

$$^{13}\mathrm{CCH} + \mathrm{H} \rightleftarrows \mathrm{C}^{13}\mathrm{CH} + \mathrm{H} + \Delta E_1$$

could have a larger contribution than excitation. It has been shown in a chemical model that this exchange reaction has an important impact on the [C$^{13}$CH/$^{13}$CCH] ratio (Furuya et al. 2011). This reaction could have less impact at higher kinetic temperatures and then allow excitation mechanisms to be more competitive. Nevertheless, these explorations should be looked more carefully in a more complete radiative transfer modeling.

## ACKNOWLEDGEMENTS

We acknowledge financial support from the European Research Council (Consolidator Grant COLLEXISM, Grant Agreement No. 811363). We wish to acknowledge the support from the CEA/GENCI (Grand Equipement National de Calcul Intensif) for awarding us access to the TGCC (Très Grand Centre de Calcul) Joliot Curie/IRENE supercomputer within the A0110413001 project. We also acknowledge Guillaume Raffy and Benjamin Desrousseaux for recent and wide improvements on the HIBRIDON scattering code to make it suitable for this work.

## DATA AVAILABILITY

The computed collisional data for both $^{13}$CCH–*sph*-$H_2$ and C$^{13}$CH–*sph*-$H_2$ will be available on the following databases: BASECOL (Dubernet et al. 2012), LAMDA (Van der Tak et al. 2020) and EMAA (Faure et al. 2021)

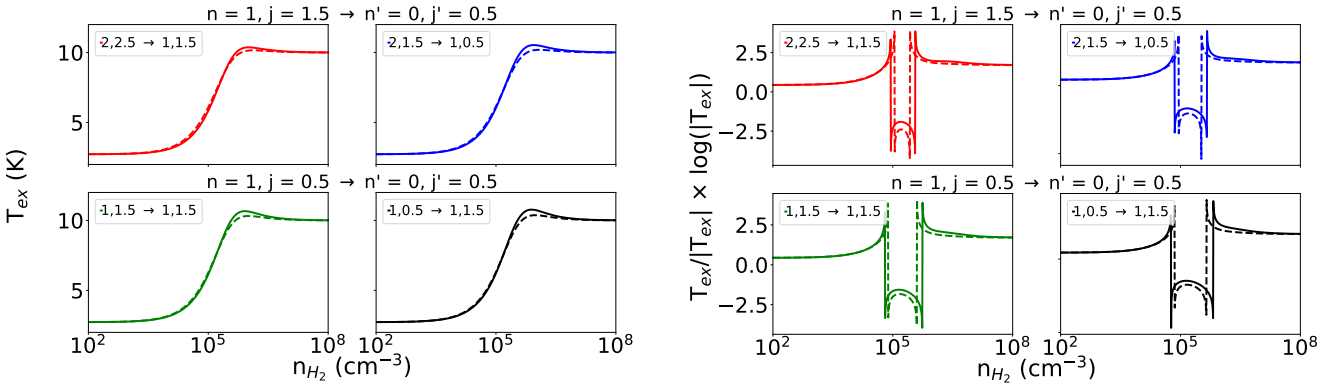


**Figure 7.** $H_2$ density dependence of excitation temperatures for selected hyperfine transitions of $^{13}$CCH (dashed lines) and C$^{13}$CH (solid lines) for $T_{\rm kin}$ = 10 K (left) and $T_{\rm kin}$ = 50 K (right). The numbers in legend correspond to the $F_1, F \rightarrow F_1', F'$ quantum numbers

**Table 2.** Comparison of ratio of brightness temperatures $T_{\rm B}$ (in mK) of $^{13}$CCH and C$^{13}$CH for several hyperfine transitions

| Transition | | Ratio of $T_{\rm B}$ | | | |
|---|---|---|---|---|---|
| $(n, j, F_1, F) \rightarrow (n', j', F_1', F')$ | $n_{\rm H_2}$ (cm$^{-3}$) | $T_{\rm kin}$ = 10 K | $T_{\rm kin}$ = 30 K | $T_{\rm kin}$ = 50 K | Ratio of $A_{ul}$ |
| (1,1.5,2,2.5) → (0,0.5,1,1.5) | $3 \times 10^4$ | 0.92 | 0.98 | 1.00 | |
| | $3 \times 10^5$ | 1.03 | 1.05 | 1.05 | |
| | LTE | 1.02 | 1.02 | 1.02 | 1.04 |
| (1,1.5,2,1.5) → (0,0.5,1,0.5) | $3 \times 10^4$ | 0.98 | 1.04 | 1.06 | |
| | $3 \times 10^5$ | 1.07 | 1.09 | 1.09 | |
| | LTE | 1.05 | 1.05 | 1.04 | 1.07 |
| (1,0.5,1,0.5) → (0,0.5,1,1.5) | $3 \times 10^4$ | 1.33 | 1.42 | 1.45 | |
| | $3 \times 10^5$ | 1.42 | 1.46 | 1.46 | |
| | LTE | 1.39 | 1.38 | 1.38 | 1.41 |
| (1,0.5,0,0.5) → (0,0.5,1,0.5) | $3 \times 10^4$ | 1.29 | 1.36 | 1.39 | |
| | $3 \times 10^5$ | 1.40 | 1.43 | 1.42 | |
| | LTE | 1.38 | 1.38 | 1.37 | 1.41 |
| (2,1.5,1,1.5) → (1,0.5,1,0.5) | $3 \times 10^4$ | ... | 1.32 | 1.33 | |
| | $3 \times 10^5$ | ... | 1.44 | 1.45 | |
| | LTE | ... | 1.47 | 1.47 | 1.50 |

## REFERENCES


Alexander M. H., 1982, J. Chem. Phys., 76
Alexander M. H., Dagdigian P. J., 1985, J. Chem. Phys., 83, 2191
Alexander M. H., Dagdigian P. J., Werner H. J., Kłos J., Desrousseaux B., Raffy G., Lique F., 2023, Computer Physics Communications, XXX, xxx
Beuther H., Semenov D., Henning Th., Linz H., 2008, ApJ, 675, 33
Corey G. C., McCourt F. R., 1983, J. Chem. Phys., 87, 2723
Cuadrado S., Goicoechea J. R., Pilleri P., Cernicharo J., Fuente A., Joblin C., 2015, A&A, 575
Dagdigian P. J., 2018a, J. Chem. Phys., 148
Dagdigian P. J., 2018b, Mon. Not. R. Astronom. Soc., 479, 3227
Dagdigian P. J., 2019, Mon. Not. R. Astronom. Soc., 487, 3427
Dagdigian P. J., 2021, Mon. Not. R. Astronom. Soc., 505, 1987
Daniel F., Dubernet M. L., Meuwly M., Cernicharo J., Pagani L., 2005, Mon. Not. R. Astronom. Soc., 363, 1083
Dubernet et al. M. L., 2012, A&A, 553, 50
Dumouchel F., Kłos J., Toboła R., Bacmann A., Maret S., Hily-Blant P., Faure A., Lique F., 2012, J. Chem. Phys., 137, 114306
Dumouchel F., Lique F., Spieldiedel A., Feautrier N., 2017, Mon. Not. R. Astronom. Soc., 471, 1849
Dutrey A., Guilloteau S., Guélin M., 1996, Chemistry of Protosolar-like Nebulae: The Molecular Content of the DM Tau and GG Tau Disks
Endres C. P., Schlemmer S., Schilke P., Stutzki J., Müller H. S. P., 2016, Journal of Molecular Spectroscopy, 327, 95
Faure A., Lique F., 2012, Mon. Not. R. Astronom. Soc., 425, 740
Faure A., Bacmann A., Boutherin B., Jacquot R., 2021, UGA, CNRS, CNRS-INSU, OSUG
Flower D. R., Lique F., 2015, Mon. Not. R. Astronom. Soc., 446, 1750
Furuya K., Aikawa Y., Sakai N., Yamamoto S., 2011, ApJ, 731
Goldflam R., Kouri D. J., Green S., 1977, J. Chem. Phys., 67, 5661
Gottlieb C. A., Gottlieb E. W., Thaddeus P., 1983, ApJ, 264, 740
Green S., Thaddeus P., 1974, ApJ, 191, 653
Kalugina Y., Lique F., Kłos J., 2012, Mon. Not. R. Astronom. Soc., 422, 812
Kłos J., Dagdigian P. J., Alexander M. H., Faure A., Lique F., 2020, Mon. Not. R. Astronom. Soc., 493, 3491
Knowles P. J., Hampel C., Werner H. J., 1993, J. Chem. Phys., 99, 5219
Lara-Moreno M., Stoecklin T., Halvick P., 2021, Mon. Not. R. Astronom.

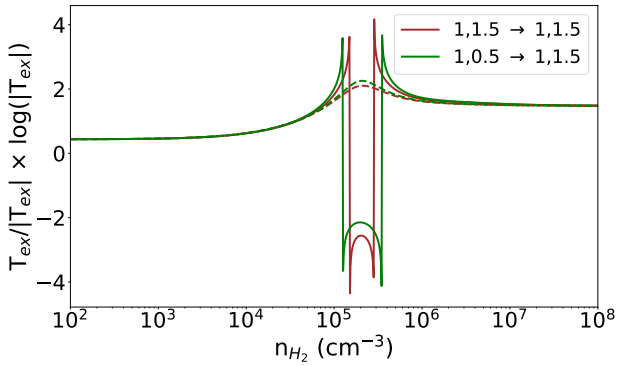


**Figure 8.** Excitation temperatures for the $n = 1$, $j = 0.5 \rightarrow n' = 0$, $j' = 0.5$ hyperfine transitions of $^{13}$CCH (dashed lines) and C$^{13}$CH (solid lines) for $T_{\rm kin} = 30$ K. The numbers in legend correspond to the $F_1, F \rightarrow F'_1, F'$ quantum numbers


Soc., 507, 4086
Loreau J., Lique F., Faure A., 2018, ApJL, 853, 5
Lucas R., Liszt H., 1998, A&A, 337, 246
McCarthy M. C., Gottlieb C. A., Thaddeus P., 1995, Journal of Molecular Spectroscopy, 173, 303
Neufeld D. A., Green S., 1994, ApJ, 432, 158
Offer A. R., van Hemert M. C., van Dishoeck E. W., 1993, J. Chem. Phys., 100
Padovani M., Walmsley C. M., Tafalla M., Galli D., Müller H. S. P., 2009, A&A, 505, 1199
Pirlot Jankowiak P., Kalugina Y., Ramachandran R., Raffy G., Dagdigian P. J., Lique F., 2021, J. Chem. Phys., 155
Sakai N., Saruwatari O., Sakai T., Takano S., Yamamoto S., 2010, A&A, 512
Salek A. H., Simon R., Winnewisser G., Wouterloot J. G. A., 1994, Can. J. Phys., 72
Sastry K. V. L. N., Helminger P., Charo A., Herbst E., De Lucia F. C., 1981, ApJ, 251, 119
Taniguchi K., Herbst E., Ozeki H., Saito M., 2019, ApJ, 884
Teyssier D., Fossé D., Gerin M., Pety J., Abergel A., Roueff E., 2003, A&A, 417, 135
Tucker K. D., Kutner M. L., Thaddeus P., 1974, ApJ, 193, 115
Van der Tak F. F. S., Black J. H., Schöier F. L., Jansen D. J., van Dishoeck E. F., 2007, Mon. Not. R. Astronom. Soc., 468, 627
Van der Tak F. F. S., Lique F., Faure A., Black J. H., van Dishoeck E. F., 2020, Atoms, 8, 15
Yoshida K., Sakai N., Nishimura Y., Tokumode T., Watanabe Y., Sakai T., Takano S., 2019, Publ. Astron. Soc. Japan, 71
Ziurys L. M., Saykally R. J., Plambeck R. L., Erickson N. R., 1982, ApJ, 254, 94


## APPENDIX A: INFINITE ORDER SUDDEN LIMIT

The IOS method can be applied if the collision energy is larger than the rotational spacings, and hence the rotational motion can be neglected (Goldflam et al. 1977). In this case, it is possible to employ the transitions out of the lowest rotational level $j = 0$ to derive hyperfine resolved rate coefficients for the targeted isotopologue. This approach has been generalized by Alexander (1982) for the case of a linear molecule in a $^2\Sigma^+$ electronic state

$$
\begin{aligned}
k^{\rm IOS}_{njF\rightarrow n'j'F'} &= [j][j'][F']\sum_L \frac{[L]}{L+1} \\
&\times \begin{pmatrix} j' & L & j \\ -\frac{1}{2} & 0 & \frac{1}{2} \end{pmatrix}^2 \begin{Bmatrix} j & j' & L \\ F' & F & I({\rm H}) \end{Bmatrix}^2 \\
&\times \frac{1}{2}[1+\epsilon(-1)^{j+j'+L}]k^{\rm CC}_{0,\frac{1}{2}\rightarrow L,L+\frac{1}{2}} \qquad \text{(A1)}
\end{aligned}
$$

where $|j - j'| < L < j + j'$ and $\epsilon$ is the parity index.

For the purpose of this work, Eq. A1 has been adapted to take into account one nuclear spin and where $k^{\rm IOS}_{0,\frac{1}{2}\rightarrow L,L+\frac{1}{2}}$ have been replaced by the exact fundamental transitions $k^{\rm CC}_{0,\frac{1}{2}\rightarrow L,L+\frac{1}{2}}$ as is can be seen in earlier work (Daniel et al. 2005; Faure & Lique 2012).

One issue is that for low collisional energies, spacings between rotational energy levels are not negligible. This approximation is expected to fail at low temperature. Neufeld & Green (1994) suggested a scaling procedure to provide a correction at low temperature

$$
k^{\rm NG}_{njF\rightarrow n'j'F'}(T) = \frac{k^{\rm IOS}_{njF\rightarrow n'j'F'}(T)}{k^{\rm IOS}_{nj\rightarrow n'j'}(T)} k^{\rm CC}_{nj\rightarrow n'j'}(T) \qquad \text{(A2)}
$$

This scaling relation satisfies the condition

$$
\sum_{F'} k^{\rm NG}_{njF\rightarrow n'j'F'}(T) = k^{\rm CC}_{nj\rightarrow n'j'}(T) \qquad \text{(A3)}
$$

However, this correction needs converged CC elastic transitions in order to provide hyperfine quasi-elastic transitions ($n = n', j = j', F \neq F'$), which is usually not the case in scattering calculations. Then, this correction is not suitable to describe such transitions.

## APPENDIX B: DETAILS ABOUT THE CONVERGED PARAMETERS USED IN SCATTERING CALCULATIONS

In order to determine accurate cross sections in scattering calculations, it is necessary to optimize the parameters used in the CC equations. We provide in Table B1 the rotational basis of the target $n_{\rm max}$, the largest total angular momentum $J_{\rm TOT}$ and the step $\Delta$E between total energies intervals $E_{\rm TOT}$. The neglect of the structure of $H_2$ imply that rotational basis of $H_2$ is chosen as $j_2 = 0$ and its rotational constant omitted. For both collisional systems, the radial propagation was considered between $R_{\rm min} = 4.25a_0$ and $R_{\rm max} = 60a_0$. Each parameter has been determined to ensure converged cross sections within 1% of deviation. Hyperfine calculations were then computed using the nuclear spin-free $S$-matrices determined with these convergence parameters.

This paper has been typeset from a TEX/LATEX file prepared by the author.

| | | $^{13}$CCH–*sph*-$H_2$ | | C$^{13}$CH–*sph*-$H_2$ | |
|---|---|---|---|---|---|
| $E_{TOT}$ (cm$^{-1}$) | $\Delta$E (cm$^{-1}$) | $n_{max}$ | $J_{TOT}$ | $n_{max}$ | $J_{TOT}$ |
| 0.1 - 50 | 0.1 | 10 | 18 | 11 | 15 |
| 50 - 100 | 0.1 | 12 | 24 | 11 | 24 |
| 100 - 200 | 0.1 | 16 | 30 | 15 | 30 |
| 200.5 - 500 | 0.5 | 22 | 45 | 22 | 42 |
| 501 - 700 | 1 | 24 | 51 | 23 | 48 |
| 705 - 1000 | 5 | 27 | 57 | 27 | 54 |
| 1010 - 1370 | 10 | 33 | 63 | 32 | 60 |

**Table B1.** Rotational basis set $n_{max}$ and optimized total angular momentum $J_{TOT}$ used for scattering calculations. These parameters are chosen for several total energies $E_{TOT}$ with different steps $\Delta$E.